NACA

RESEARCH MEMORANDUM

EXPERIMENTAL DRAG COEFFICIENTS OF ROUND NOSES WITH CONICAL WINDSHIELDS AT MACH NUMBER 2.72

By Jim J. Jones

Langley Aeronautical Laboratory
Langley Field, Va.

NATIONAL ADVISORY COMMITTEE
FOR AERONAUTICS

WASHINGTON

June 28, 1955
Declassified May 8, 1957

NACA RM L55E10

NATIONAL ADVISORY COMMITTEE FOR AERONAUTICS

RESEARCH MEMORANDUM

EXPERIMENTAL DRAG COEFFICIENTS OF ROUND NOSES WITH CONICAL WINDSHIELDS AT MACH NUMBER 2.72

By Jim J. Jones

SUMMARY

An exploratory investigation at Mach number 2.72 has been made to show the decrease in the drag of a round-nose model achieved by mounting a small cone on a rod ahead of the nose. The geometric parameters which were varied were the cone-base diameter, cone angle, and rod length. On one model the rod was replaced by two off-axis legs.

All models showed large decreases in drag compared to that of the round nose alone.

INTRODUCTION

In many radome-type installations bluff noses, which unfortunately adversely affect the drag of otherwise efficient aerodynamic shapes, are required. In order to reduce the drag of supersonic missiles with such bluff or rounded noses, several investigations have been conducted. (See, for instance, refs. 1 to 8.) One promising method (refs. 1 to 6) is to mount a cone symmetrically on a small-diameter rod ahead of the nose. The thought behind this configuration, frequently referred to as a conical windshield, is that the wake of the cone will expand to form a conically shaped region of separated flow, thus replacing the strong detached shock wave with a conical shock wave and thereby reduce the drag. Experimentally, the actual occurrence of such a flow pattern is related to a number of variables such as the length of the rod, the cone size, and the Mach number and Reynolds number. The results of one of the most detailed and systematic investigations of flows of this type are presented in reference 4.

In 1952 some limited data on the effects of various cones on the drag of a round-nose body of revolution were obtained in the Langley gas dynamics laboratory at a Mach number of 2.72 and a Reynolds number of 1.8×10^6 per inch. These tests were of an exploratory nature; the

data are now being made available because of repeated interest shown in them.

SYMBOLS

C_D	total drag coefficient of model based on maximum frontal area
C_{D_C}	wave drag coefficient of cone alone based on maximum frontal area of model
L	length of rod from base of cone to rounded nose
r	radial coordinate of basic nose
r_n	radius of spherical nosepiece
x	axial coordinate of basic nose, measured from base
α	apex angle of nose cone

APPARATUS AND TESTS

Models

The basic nose model used for this investigation was an ogive with the tip replaced by a spherical segment tangent to the ogive (see fig. 1). The ogive before modification was designed for minimum wave drag for a fineness ratio of 4 according to the theory of reference 9. The radius of the model base was 0.5 inch and the radius of the spherical tip was 0.375 inch. The fineness ratio after modification was 2.058. The ordinates are given in figure 1.

Various cone and rod configurations were installed ahead of the basic model. These configurations are sketched in figure 1 and discussed in the following sections.

Constant cone diameter (models 1 to 4).- Four cones having a base diameter of 0.250 inch were mounted on a rod 1.125 inches long. The apex angles of the cones were 20°, 30°, 40°, and 50° (designated models 1, 2, 3, and 4, respectively). The cone length decreased with increasing apex angle.

Constant cone length (models 5 to 7).- Three cones having a cone length of 0.536 inch were mounted on a rod 1.464 inches long. The apex

angles of the cones were 30°, 40°, and 50° (designated models 5, 6, and 7, respectively). For this series, the base diameter of the cone increased with increasing apex angle.

Short rod (model 8).- One model was constructed with a small cone angle (20°) and short rod length (0.415 inch) such that the cone surface, if extended, would intersect the spherical tip of the nose. This condition would not occur for any other model.

Bipod mount (model 9).- Model 9 consisted of a cone identical to that of model 1 (α = 20°) mounted on two off-axis legs (bipod mount) which separated the cone base from the model nose by 1.125 inches. Such a configuration was tried because it might be undesirable, in some installations, to use a symmetrical rod.

Installation

The models were mounted to a strain-gage drag balance which in turn was sting mounted in the tunnel. The shield over the balance had the same diameter as the model base and approached to within 1/32 inch of the model. The base pressure was measured in this gap by an orifice and this pressure was used in correcting the data to the condition of zero base drag on the model.

Tests

All models were tested at zero angle of attack at a Mach number of 2.72 and a Reynolds number of 1.83×10^6 per inch. The test section of the tunnel measured 3 inches by 5 inches. For comparison purposes the basic nose, without rod, was also tested at the same conditions.

RESULTS AND DISCUSSION

The drag coefficients obtained for all models are:

Model	1	2	3	4	5	6	7	8	9	Basic nose
C_D	0.156	.175	.181	.196	.370	.194	.240	.236	.188	.550
$\frac{(C_D)_{model}}{(C_D)_{basic\ nose}}$	0.284	.319	.329	.357	.673	.353	.437	.430	.342	

The drag coefficients of models 1 to 4 and models 5 to 7 are plotted against cone angle in figures 2(a) and 2(b), respectively. Figure 3 is a shadowgraph of the flow over the basic nose, showing the strong detached shock wave.

All rod configurations resulted in large decreases in drag from the basic nose. The lowest drag coefficient, which occurred for model 1, was only 28 percent of that for the basic nose. Model 1, however, does not necessarily represent the optimum for these test conditions inasmuch as no special attempt was made to find such an optimum. These drag reductions would of course not be as large percentagewise if consideration were given to the total drag of a complete missile, with the accompanying drag of the base, control surfaces, increased skin friction, and so forth.

Constant-cone-diameter model.- The drag coefficients of the constant-cone-diameter models (models 1 to 4) are plotted in figure 2(a) as a function of cone angle; corresponding shadowgraphs are presented in figures 4 to 7. Included in figure 2(a) are the drag values obtained by subtracting the cone wave drag from the total drag. From these curves, it is evident that about half the variations in total drag of the cone—basic-nose combination is due to the variation in wave drag of the nose cone, the remainder being associated with the separated region. It is interesting to note in the shadowgraphs (figs. 4 to 7) that there is no discernible difference in the slope of the separated region boundary or the shape of the shock wave near the rounded nose.

Constant-cone-length model.- The drag coefficients of the constant-cone-length models (models 5 to 7) are plotted in figure 2(b) as a function of cone angle; corresponding shadowgraphs are presented in figures 8 to 10. As in figure 2(a), the drag values obtained by subtracting the cone wave drag from the total drag are included. From figure 2(b) it can be seen that models 6 and 7 have considerable less drag than model 5, with the difference between models 6 and 7 being primarily the wave drag of the nose cone. The high drag of model 5 (the highest drag of any of the rod configurations) can be attributed (fig. 8) to the excessive rod length (for a given nose cone) and hence the flow reattachment to the rod. This flow attachment defeats the purpose of the cone. For this configuration (model 5), there is little interaction of the blunt body on the separated flow immediately behind the nose cone. The theoretical prediction of whether or not flow reattachment on the rod will occur seems an insurmountable task in that it depends on the rod length, cone diameter and angle, type of boundary layer on the cone, and so forth for any given bluff body. It is interesting to note that on model 2, which is essentially model 5 with a shorter rod, the flow does not reattach but remains fully separated. If the flow were to reattach on model 2, the reattachment point on the rod would be closer to the body and to the separated region just ahead

of the body. It is concluded that it is the proximity of the reattachment point to the point of separation and their mutual interference that prevents flow reattachment on model 2.

Short-rod model.- The short-rod model (model 8) is an example of a configuration in which the cone angle is not as great as the slope of the mixing boundary (fig. 11). The pressure in the separated region is probably greater than that on the cone surface. This high back pressure therefore feeds up into the boundary layer on the cone and separates it before it reaches the rear of the cone. This separation on the cone surface may be seen in figure 11. Thus, this flow pattern is not essentially different from that for the spike-alone configurations of references 7 and 8.

Bipod-mount model.- The bipod-mount model (model 9), which supported the cone on two off-axis legs (shown in side view in fig. 12), had a drag coefficient 20 percent higher than that measured for model 1. This would indicate that replacing the axially located rod with a number of off-axis legs adds materially to the drag coefficient.

CONCLUDING REMARKS

A brief exploratory investigation at a Mach number of 2.72 indicated that sizable reductions in the drag of a round-nose model may be achieved by mounting a small cone on a rod ahead of the model. The lowest drag configuration tested had a drag coefficient that was 28 percent of that for the rounded nose alone.

Two general types of flow patterns were observed. In one type the flow reattached to the rod behind the cone and then separated again from the rod ahead of the round nose. This flow pattern, which resulted in a high drag configuration, was associated with an excessive rod length for the given cone size. For the second type of flow pattern, which was observed for all configurations tested except one, the flow detached at the rear of the cone, remained separated over the entire rod length, and reattached near the rim of the round nose. Configurations with this type of flow pattern showed large drag decreases.

Langley Aeronautical Laboratory,
National Advisory Committee for Aeronautics,
Langley Field, Va., April 21, 1955.

REFERENCES

1. Alexander, Sidney R.: Results of Tests To Determine the Effect of a Conical Windshield on the Drag of a Bluff Body at Supersonic Speeds. NACA RM L6K08a, 1947.

2. Alexander, Sidney R., and Katz, Ellis: Flight Tests To Determine the Effect of Length of a Conical Windshield on the Drag of a Bluff Body at Supersonic Speeds. NACA RM L6J16a, 1947.

3. Alexander, Sidney R.: Flight Investigations at Low Supersonic Speeds To Determine the Effectiveness of Cones and a Wedge in Reducing the Drag of Round-Nose Bodies and Airfoils. NACA RM L8L07a, 1949.

4. Beastall, D., and Turner, J.: The Effect of a Spike Protruding in Front of a Bluff Body at Supersonic Speeds. TN No. Aero. 2137, British R.A.E., Jan. 1952.

5. Piland, Robert O.: Preliminary Free-Flight Investigation of the Zero-Lift Drag Penalties of Several Missile Nose Shapes for Infrared Seeking Devices. NACA RM L52F23, 1952.

6. Robins, A. Warner: Preliminary Investigations of the Effect of Several Seeker-Nose Configurations on the Longitudinal Characteristics of a Canard-Type Missile at a Mach Number of 1.60. NACA RM L53I18, 1953.

7. Moeckel, W. E.: Flow Separation Ahead of a Blunt Axially Symmetric Body at Mach Numbers 1.76 to 2.10. NACA RM E51I25, 1951.

8. Jones, Jim J.: Flow Separation From Rods Ahead of Blunt Noses at Mach Number of 2.72. NACA RM L52E05a, 1952.

9. Von Kármán, Th.: The Problem of Resistance in Compressible Fluids. Atti del v Convegno della Fondazione Alessandro Volta, R. Accad. d'Italia, vol. XIV, 1936, pp. 5-59.

Ordinates for basic nose

x	r	x	r
0	0.500	1.30	0.424
.10	.498	1.40	.415
.20	.495	1.50	.405
.30	.491	1.60	.395
.40	.487	1.70	.386
.50	.482	1.80	.365
.60	.476	1.85	.343
.70	.469	1.90	.310
.80	.463	1.95	.270
.90	.456	2.00	.202
1.00	.449	2.03	.194
1.10	.440	2.05	.175
1.20	.432	2.058	0

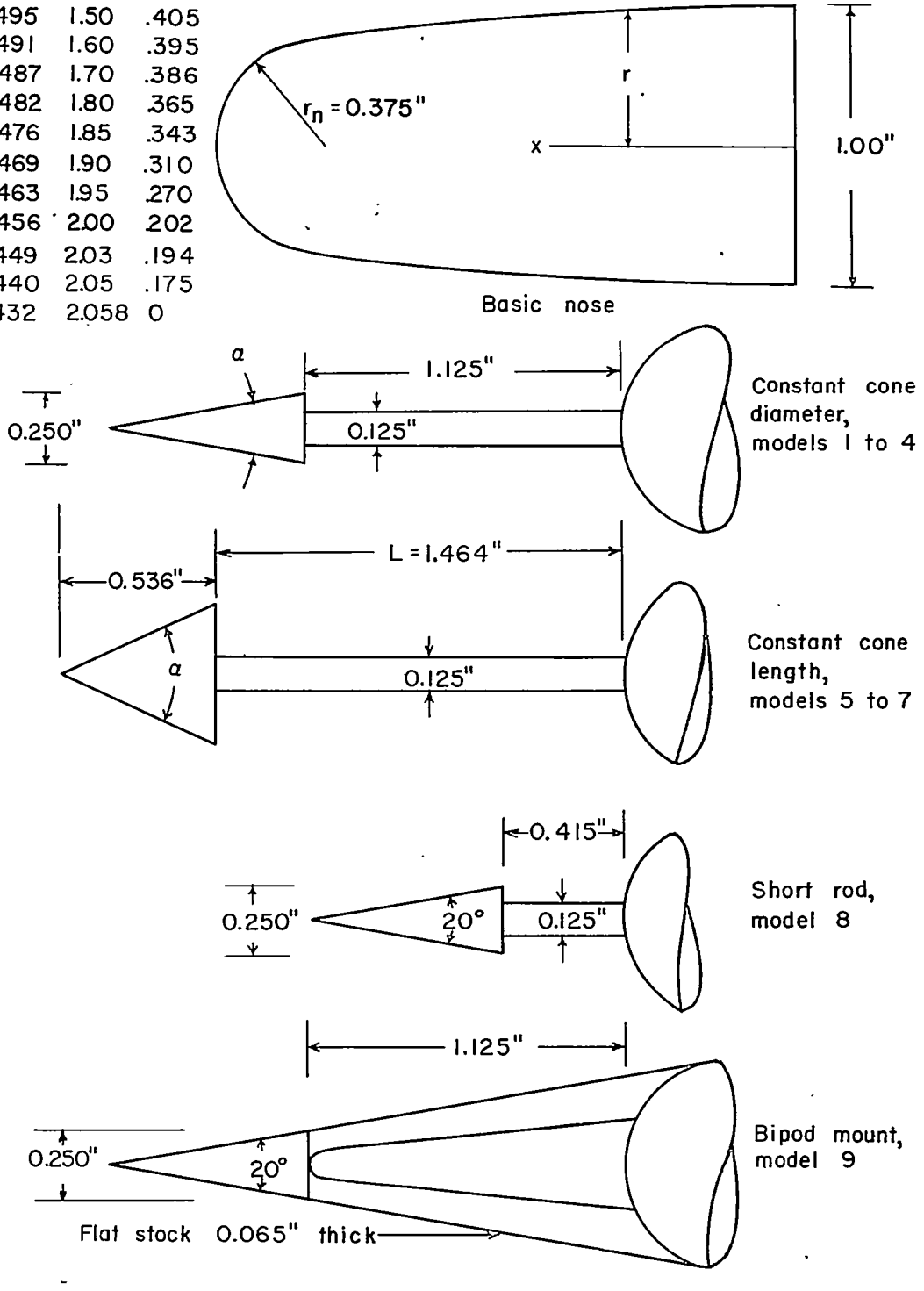

Figure 1.- Sketch of models tested.

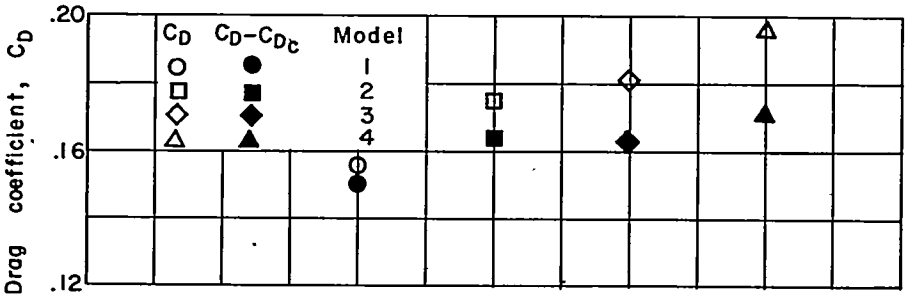

(a) Constant-cone-diameter series.

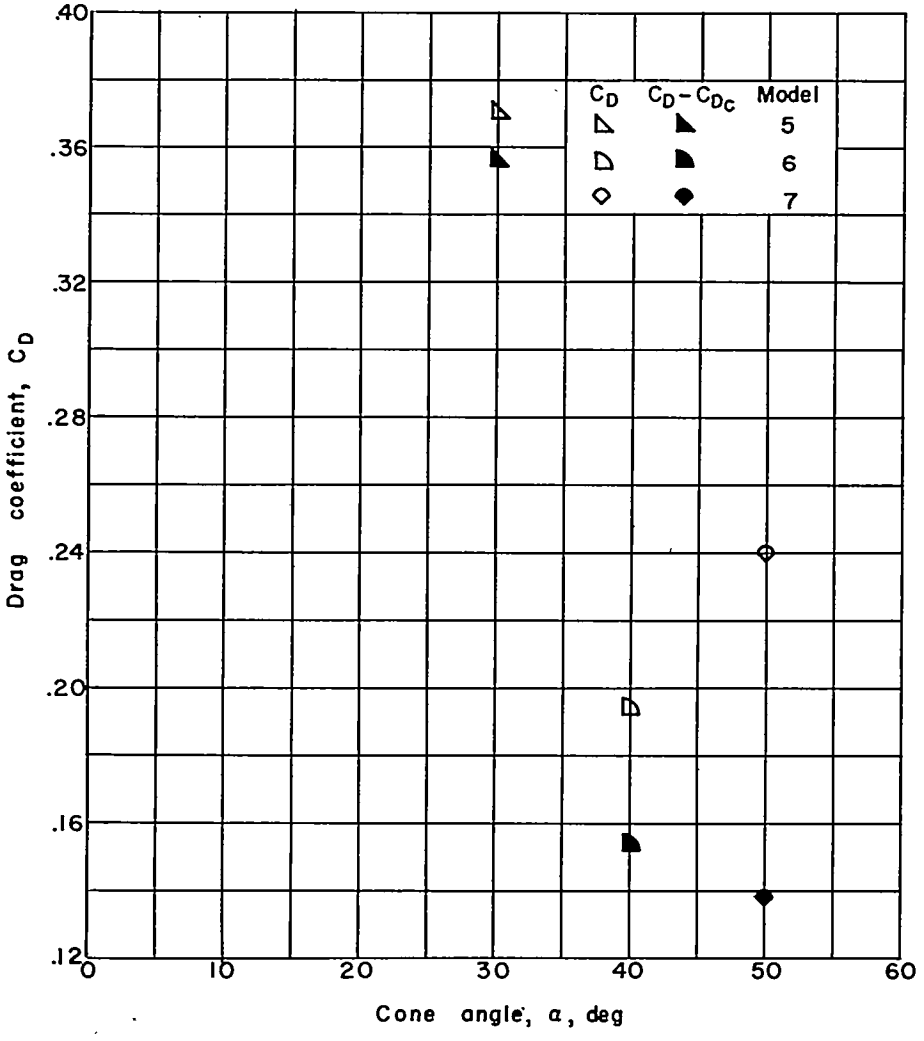

(b) Constant-cone-length series.

Figure 2.- Drag coefficient plotted against cone angle.

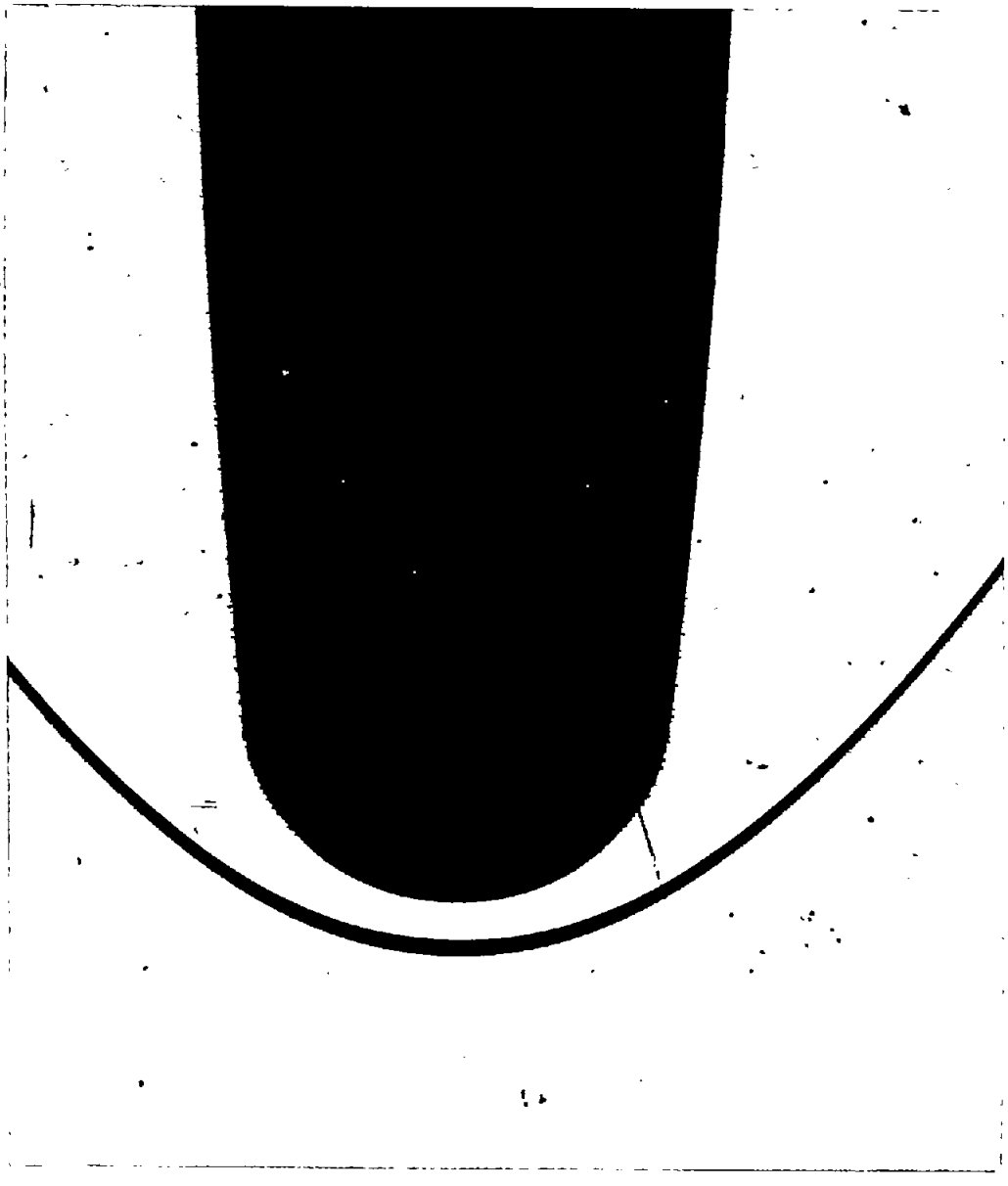

L-87951

Figure 3.- Shadowgraph of flow over basic nose.

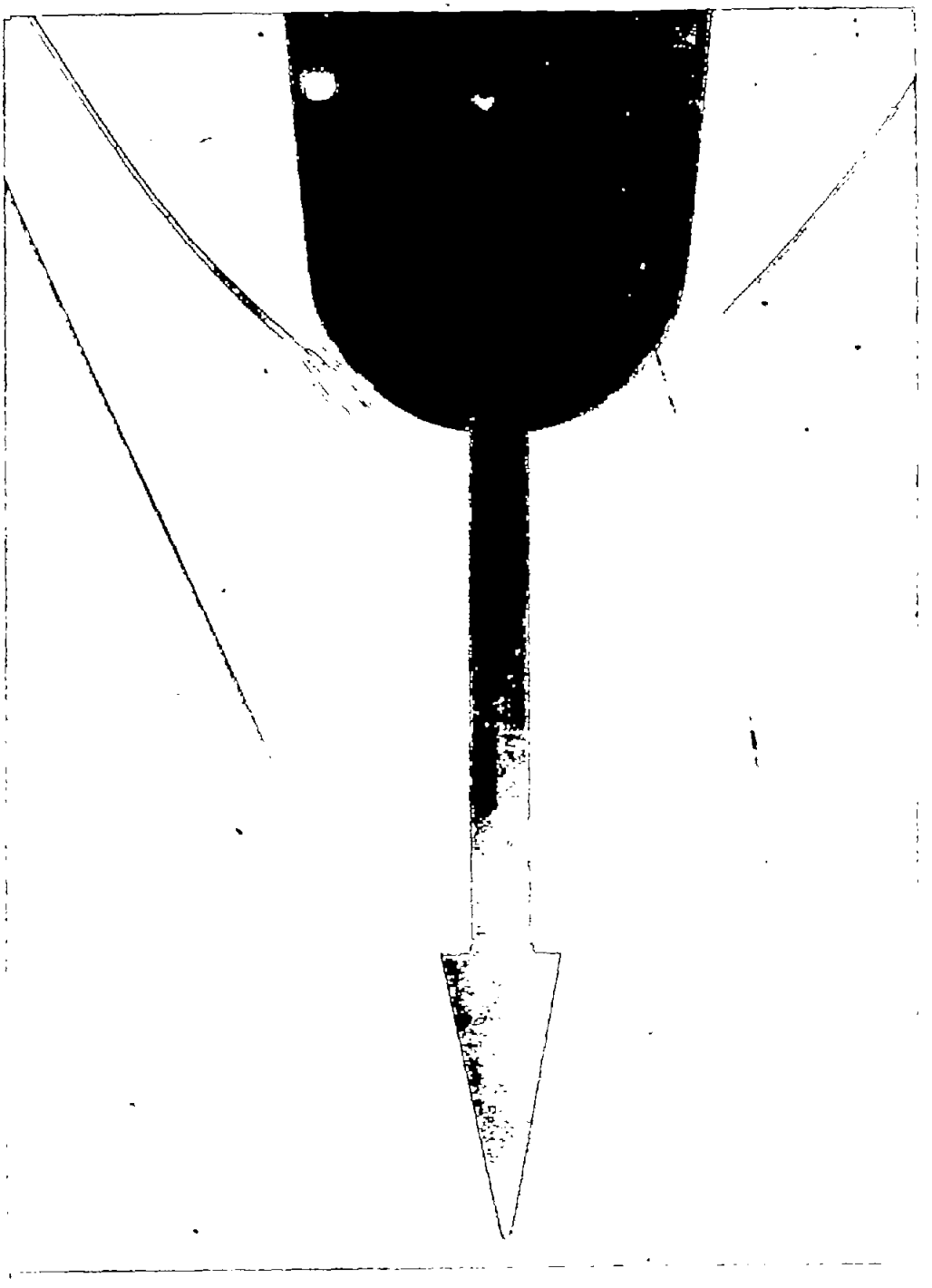

L-87952

Figure 4.- Shadowgraph of model 1, $\alpha = 20^{\circ}$.

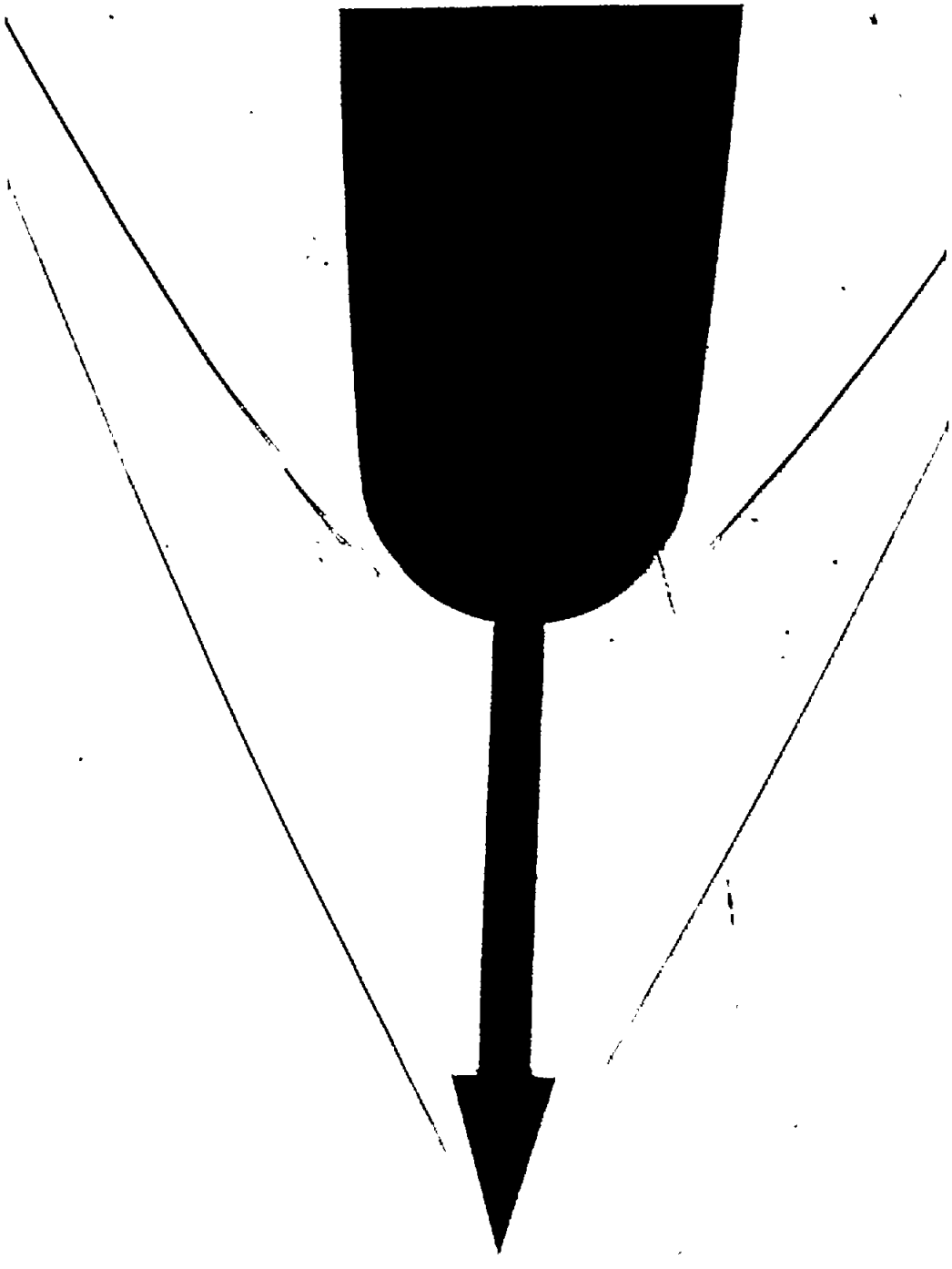

L-87953

Figure 5.- Shadowgraph of model 2, $\alpha = 30^{\circ}$.

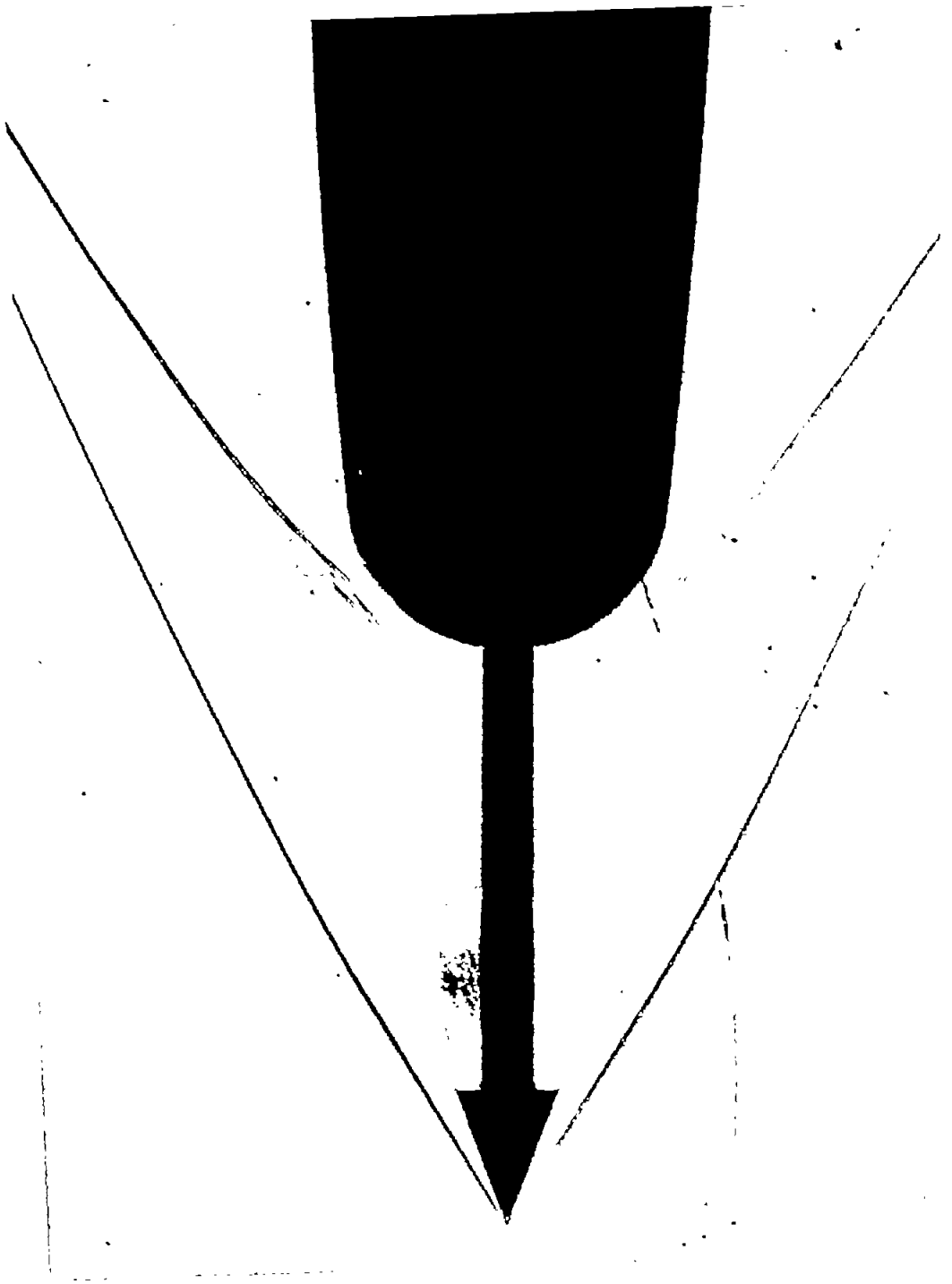

L-87954

Figure 6.- Shadowgraph of model 3, $\alpha = 40^{\circ}$.

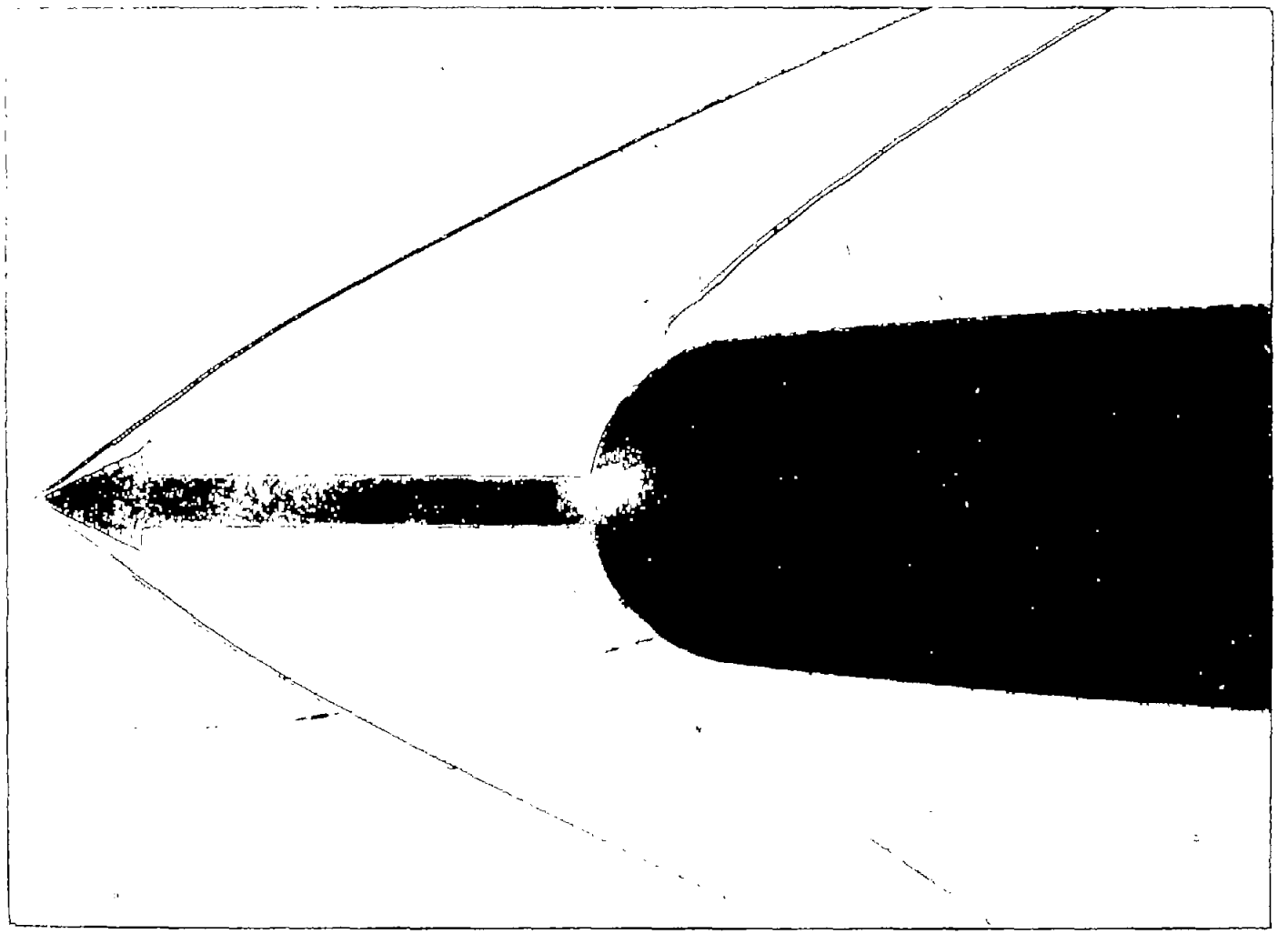

L-87955

Figure 7.- Shadowgraph of model 4, $\alpha = 50^{\circ}$.

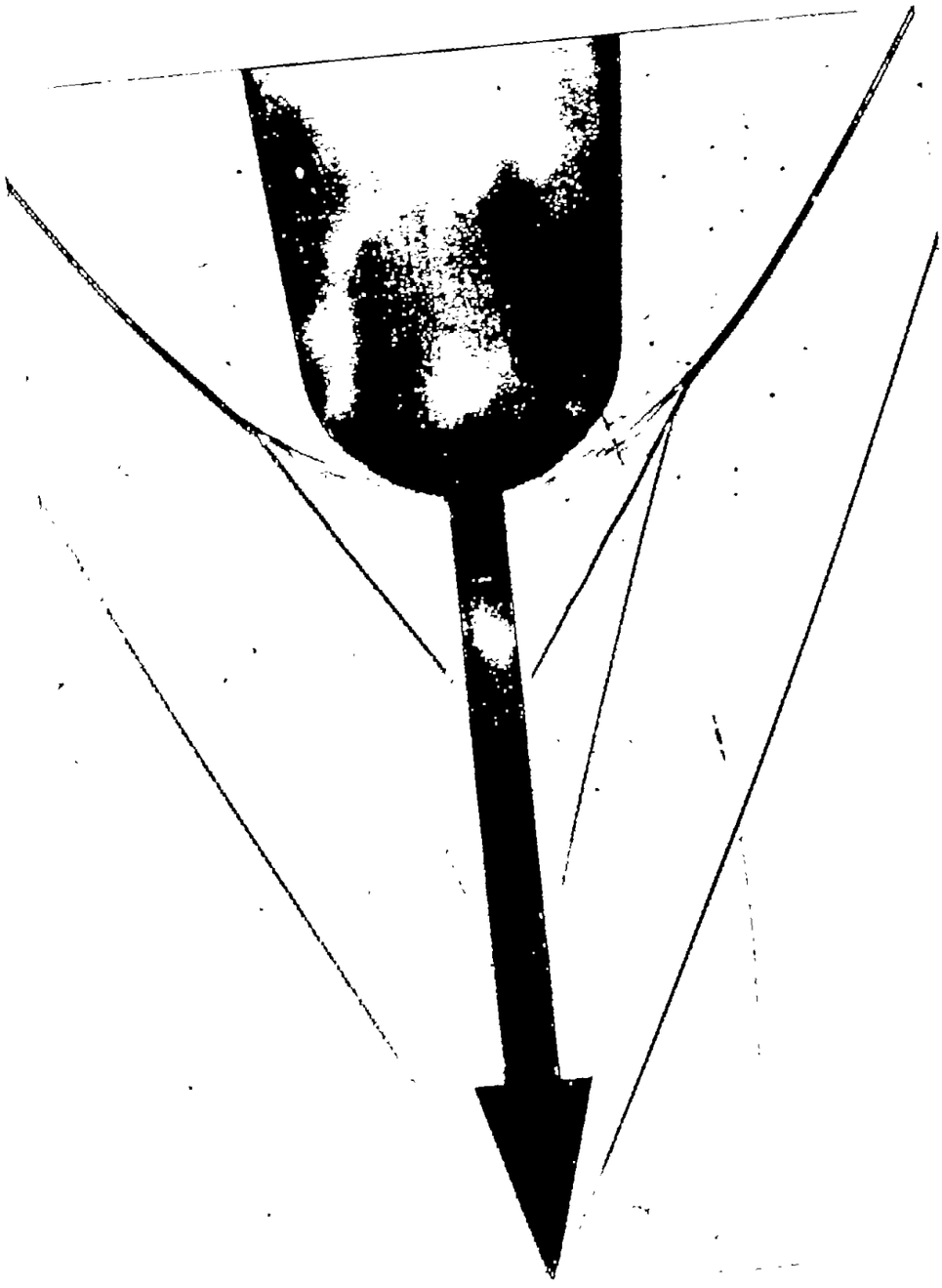

L-87956

Figure 8.- Shadowgraph of model 5, $\alpha = 30^{\circ}$.

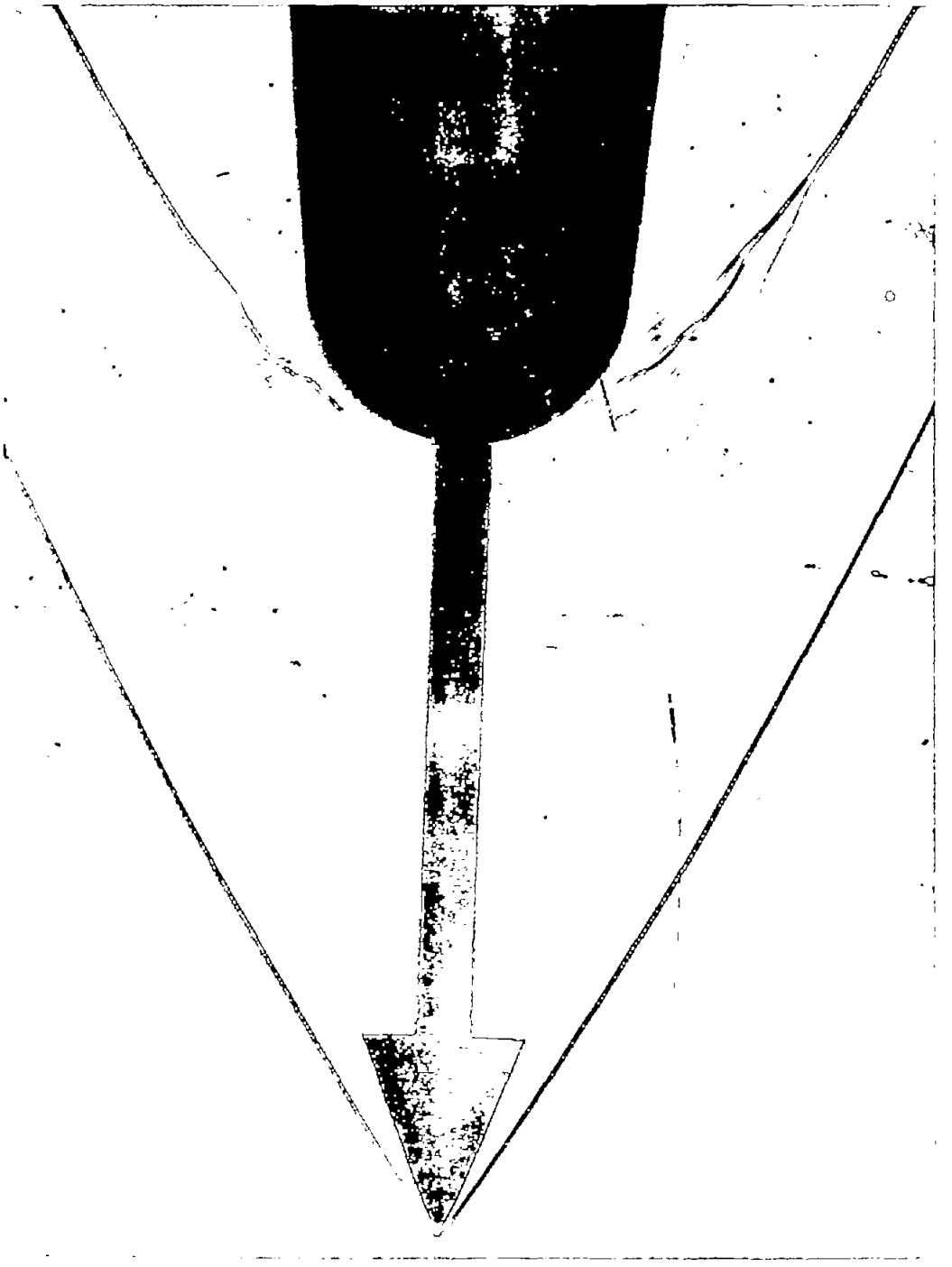

L-87957

Figure 9.- Shadowgraph of model 6, $\alpha = 40^{\circ}$.

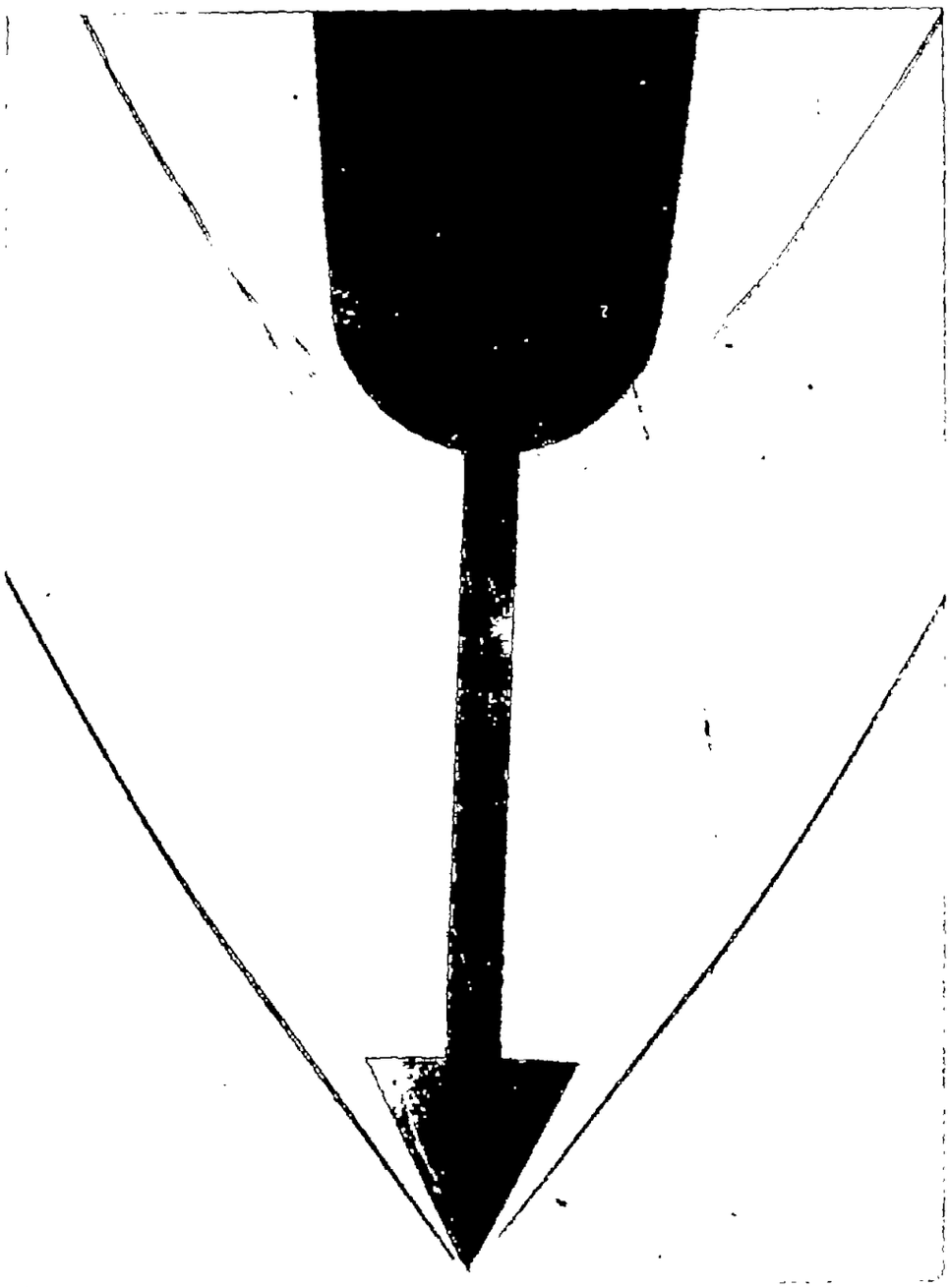

L-87958

Figure 10.- Shadowgraph of model 7, $\alpha = 50^{\circ}$.

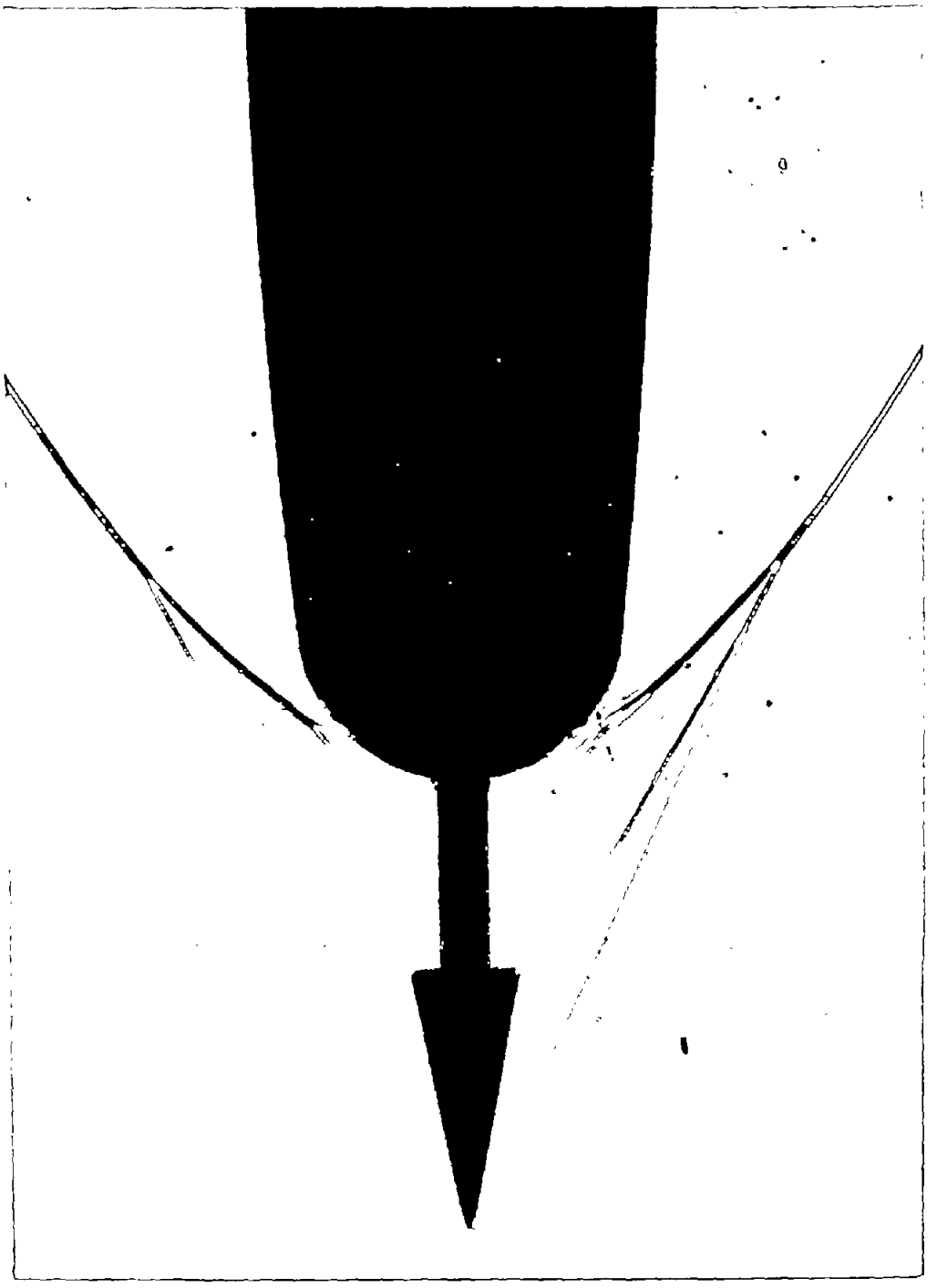

L-87959

Figure 11.- Shadowgraph of model 8, $\alpha = 20^{\circ}$.

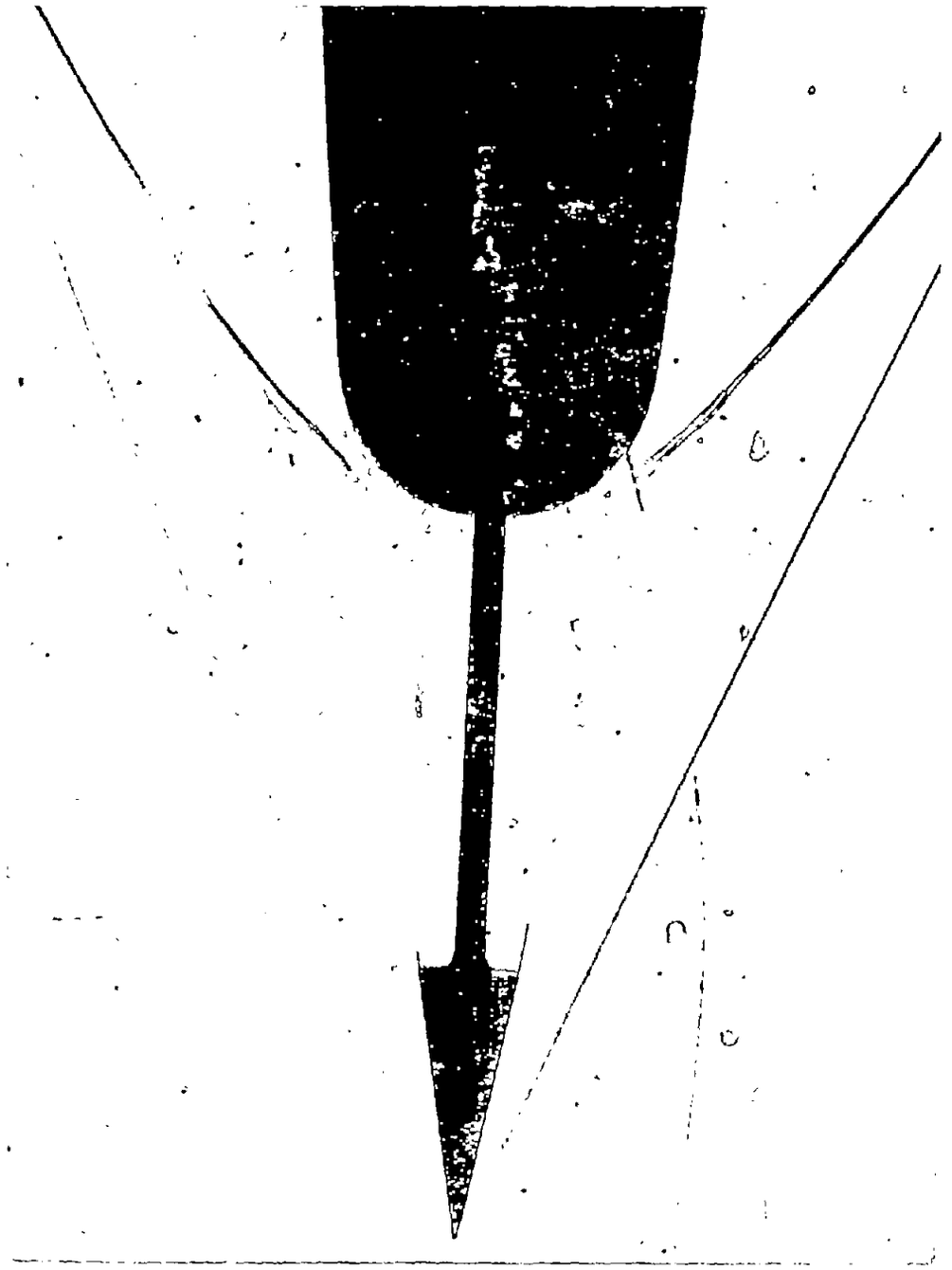

L-87960

Figure 12.- Shadowgraph of model 9, $\alpha = 20^{\circ}$.